

Soliton Confinement in a Quantum Circuit

Ananda Roy^{1,*} and Sergei Lukyanov^{1,†}

¹Department of Physics and Astronomy, Rutgers University, Piscataway, NJ 08854-8019 USA

Confinement of topological excitations into particle-like states - typically associated with theories of elementary particles - are known to occur in condensed matter systems, arising as domain-wall confinement in quantum spin chains. However, investigation of confinement in the condensed matter setting has rarely ventured beyond lattice spin systems. Here, we analyze the confinement of sine-Gordon solitons into mesonic bound states in a one-dimensional, quantum electronic circuit (QEC) array, constructed using experimentally-demonstrated circuit elements: Josephson junctions, capacitors and $0 - \pi$ qubits. The interactions occurring naturally in the QEC array, due to tunneling of Cooper-pairs and pairs of Cooper-pairs, give rise to a non-integrable, interacting, lattice model of quantum rotors. In the scaling limit, the latter is described by the quantum sine-Gordon model, perturbed by a cosine potential with a different periodicity. We compute the string tension of confinement of sine-Gordon solitons and the changes in the low-lying spectrum in the perturbed model. The scaling limit is reached faster for the QEC array compared to conventional spin chain regularizations, allowing high-precision numerical investigation of the strong-coupling regime of this non-integrable quantum field theory. Our results, obtained using the density matrix renormalization group method, could be verified in a quench experiment using state-of-the-art QEC technologies.

Confinement and asymptotic freedom are paradigmatic examples of non-perturbative effects in strongly interacting quantum field theories (QFTs) [1]. While typically associated with theories of elementary particles [2, 3], confinement of excitations into particle-like states occurs in a wide range condensed matter systems. In the latter setting, the “hadrons” are formed due to confinement of domain walls in quantum spin chains. They have been detected using neutron scattering experiments in a coupled spin-1/2 chains [4] and in a one-dimensional Ising ferromagnet [5]. Furthermore, signatures of confinement have been observed in numerical investigations of quenches in quantum Ising spin chains [6, 7] as well as in noisy quantum simulators [8, 9].

Despite its ubiquitousness, in the condensed matter setting, quantitative investigation of confinement has rarely ventured beyond lattice spin systems. In this work, we show that confinement of topological excitations can arise in a one-dimensional, superconducting, quantum electronic circuit (QEC) array. The QEC array is constructed using experimentally-demonstrated quantum circuit elements: Josephson junctions, capacitors and $0 - \pi$ qubits [10–16]. The proposed QEC array departs from the established paradigm of probing confinement in condensed matter systems and starts with lattice quantum rotors. These lattice regularizations are particularly suitable for simulating a large class of strongly-interacting bosonic QFTs [17] due to rapid convergence to the scaling limit. While this was numerically observed in the semi-classical regime of the sine-Gordon (sG) model [18], here we show that QECs are suitable for regularizing a *strong-interacting, non-integrable* bosonic QFT.

With a specific choice of interactions that arise naturally in QEC systems due to tunneling of Cooper pairs and pairs of Cooper pairs, we verify that the long-

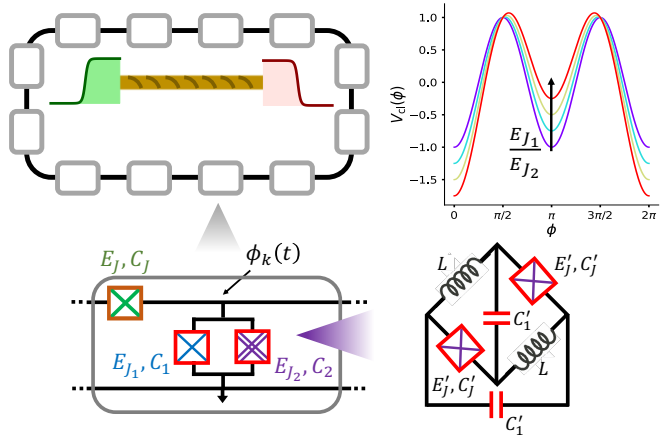


FIG. 1. Each unit cell (gray rectangle) of the QEC array contains a Josephson junction (green cross) on the horizontal link. The vertical link of the same contains a parallel circuit of an ordinary Josephson junction (blue cross) and a $\cos(2\phi)$ Josephson junction (purple crosses). The latter is formed by two Josephson junctions, two capacitors and two inductors (bottom right panel) [13]. The variation of the classical potential, V_{cl} , [Eq. (1)] as E_{J1}/E_{J2} increases from 0 in steps of $1/4$ is shown in the top right panel. For nonzero E_{J1}/E_{J2} , the solitons (green wavepacket) and anti-solitons (maroon wavepacket), interpolating between the potential minima at $\phi = 0$ and $\phi = \pi$, experience a confining potential (yellow string in top left panel), leading to the formation of mesonic bound states.

wavelength properties of the QEC array are described by a perturbed sG (psG) model [19–22]. The corresponding euclidean action is

$$\mathcal{A}_{psG} = \int d^2x \left[\frac{1}{16\pi} (\partial_\nu \varphi)^2 + V(\varphi) \right], \quad (1)$$

where $V(\varphi) = -2\mu \cos(\beta\varphi) - 2\lambda \cos(\beta\varphi/2)$ and λ, μ, β are parameters [23]. Due to the presence of the pertur-

bation $\propto \lambda$, the solitons and the antisolitons of the sG model experience a confining potential that grows linearly with their separation. This leads to the formation of mesonic excitations, analogous to the confinement phenomena occurring in the Ising model with a longitudinal field [24–29]. In the psG case, the free Ising domain-walls are replaced by interacting sG solitons. While predicted using semi-classical and perturbative analysis [20–22], quantitative investigations of confinement and any direct evidence of the psG mesons have remained elusive so far. This is performed in this work.

Each unit cell of the one-dimensional QEC array [gray rectangle in Fig. 1] contains: i) a Josephson junction on the horizontal link with junction energy (capacitance) E_J (C_J), ii) a parallel circuit of an ordinary Josephson junction [junction energy (capacitance) E_{J_1} (C_1)] and a $0 - \pi$ qubit [10–13] on the vertical link. The $0 - \pi$ qubit is realized using two Josephson junctions [junction energies (capacitances) E'_J (C'_J)], together with two inductors with inductances L [Fig. 1(b)]. In the limit $(L/C'_J)^{1/2} \gg \hbar/(2e)^2$, this circuit configuration realizes a $\cos(2\phi)$ Josephson junction [13]. In the limit $C_J \gg C_{\text{eff}}$, where $C_{\text{eff}} = C_1 + C_2$, the QEC array is described by the Hamiltonian:

$$H = E_c \sum_{k=1}^L n_k^2 + \epsilon E_c \sum_{k=1}^L n_k n_{k+1} - E_J \sum_{k=1}^L \cos(\phi_k - \phi_{k+1}) - E_g \sum_{k=1}^L n_k - \sum_{a=1,2} E_{J_a} \sum_{k=1}^L \cos(a\phi_k), \quad (2)$$

where $E_c = (2e)^2/2C_{\text{eff}}$ and we have chosen periodic boundary conditions. Here, n_k is the excess number of Cooper pairs on each superconducting island and ϕ_k is the superconducting phase at each node, satisfying $[n_j, e^{\pm i\phi_k}] = \pm \hbar \delta_{jk} e^{\pm i\phi_k}$. We approximate the exponentially-decaying, long-range interaction due to the capacitance C_J [30] with a nearest-neighbor interaction [31] of the form $\epsilon n_k n_{k+1}$, where the constant ϵ is < 1 . The third and fourth terms in Eq. (2) arise due to the coherent tunneling of Cooper-pairs between nearest-neighboring islands and due to a gate-voltage at each node. The last two cosine potentials of Eq. (2) respectively arise from tunneling of Cooper-pairs and pairs of Cooper-pairs through the Josephson junction and the $0 - \pi$ qubit on the vertical link.

For $E_{J_2} = E_{J_1} = 0$, H corresponds to a variation of the Hamiltonian of the Bose-Hubbard model [32, 33] and conserves the total number of Cooper-pairs. As E_J/E_c is increased from 0, the QEC array transitions from an insulating to superconducting phase. We focus on the superconducting phase obtained by increasing E_J/E_c at constant density [34, 35]. In the latter phase, the long-wavelength properties of the array are described by the free, compactified boson QFT [30, 31], characterized by the algebraic decay of the correlation function of the lat-

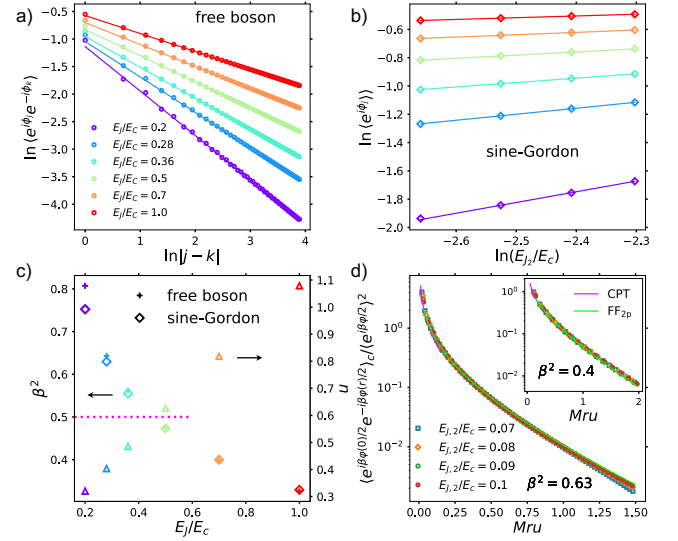


FIG. 2. DMRG results and comparison with analytical predictions. a) Verification of the power-law decay of the correlation functions of the lattice vertex operators for the free boson model. The obtained Luttinger parameter ($K = 2\beta^2$) from the slopes are plotted as pluses in c). b) Scaling of the vertex operator expectation value with E_{J_2}/E_c for the sG model. The values of the sG coupling obtained from this scaling are plotted as diamonds in c). The discrepancy between the sG result and the free-boson prediction as $\beta^2 \rightarrow 1$ occur due to corrections to scaling arising from the Kosterlitz-Thouless phase-transition occurring at $\beta^2 = 1$. The (dimensionless) Fermi velocity, u , was obtained from the Casimir energy computation of the free theory [23]. The free-fermion point of the sG model is indicated by the dotted magenta line. d) Comparison of the normalized, connected two-point correlation function of the vertex operator $e^{i\phi_j} \sim e^{i\beta\varphi/2}$ computed using DMRG and analytical computations in the repulsive ($\beta^2 \approx 0.63$) and the attractive ($\beta^2 \approx 0.4$, inset) regimes of the sG model. The ratio $1/Mu$, M being the soliton-mass, was obtained by computing the correlation length from the infinite DMRG computation.

tice vertex operator: $\langle e^{i\phi_j} e^{-i\phi_k} \rangle \propto |j - k|^{-K/2}$, where K is the Luttinger parameter. This algebraic dependence is verified in Fig. 2(a) by computing the corresponding correlation function using the density matrix renormalization group (DMRG) technique [36]. For the parameters in this work, the Luttinger parameter varies between $0 \leq K \leq 2$ [31, 37]. We further compute the dimensionless “Fermi velocity”, u , in the QEC array by analyzing the ground-state energy of the array with system-size [23] [Fig. 2(c)].

For $E_{J_2} \neq 0, E_{J_1} = 0$, keeping $E_J > E_c$, the QEC array realizes the sG model [18]. Now, the lattice model has a conserved \mathbb{Z}_2 symmetry, associated with the parity operator for the number of Cooper-pairs: $P = \prod_{k=1}^L e^{i\pi n_k}$. This symmetry leads to a two-fold degenerate ground state for this realization of the sG model. This is in contrast to the usual continuum formulation of the lat-

ter, where the ground state is one of the infinitely many vacua. The two degenerate states correspond to $\phi_k = 0$ and $\phi_k = \pi$, $k = 1, \dots, L$, with the sG solitons and anti-solitons interpolating between them. The sG coupling, β , is given by: $\beta = \sqrt{K/2} \in (0, 1)$.

We verify the sG limit of the QEC array as follows. First, we compute the scaling of the lattice operator $e^{i\phi_k}$, which, in the continuum limit, correspond to the vertex operator $e^{i\beta\phi/2}$. The scaling with the coupling E_{J_2}/E_c [Fig. 2(b)] yields the value of the sG coupling β^2 [Fig. 2(c)]. These values are compared with those expected from the free-boson computations. The discrepancy between the obtained values of β^2 for the sG and the free boson computations as $\beta^2 \rightarrow 1$ arises due to the Kosterlitz-Thouless phase-transition. We also compute the connected, two-point correlation function: $\langle e^{i\phi_j} e^{-i\phi_k} \rangle - \langle e^{i\phi_j} \rangle^2$. When normalized by $\langle e^{i\phi_j} \rangle^2$, the latter is given by a universal function, computable using analytical techniques. We compare the DMRG results with analytical predictions. We chose two representative values of β^2 to demonstrate the robustness of our results in both the attractive and repulsive regimes. The quantity, Mu , where M is the soliton mass, is obtained numerically by computing the correlation length of the lattice model using the infinite DMRG technique. The short (long) distance behavior of the normalized, connected correlation function was computed using conformal perturbation theory (form-factors [38, 39] computed by including up to two-particle contributions) [23]. The results are shown as pink (lime) solid curves labeled CPT (FF_{2p}) in Fig. 2(d).

The soliton-creating operators for the sG model [40, 41] are defined on the lattice as: $O_s^n(k) = e^{2is\phi_k} \prod_{j < k} e^{-iq\pi n_j}$, where q and s are the topological charge and the Lorentz spin of the excitations. The current QEC incarnation of the sG model gives access to solitons with $s \in \{0, 1/2, 1\}$ and $q = \pm 1$. For definiteness, we consider $s = 0$. Fig. 3(a) (empty markers) shows the energy cost, T , of separating a soliton-antisoliton pair, after they are created by application of O_s^n at two different locations for different values of β^2 . For the sG model, as expected, $T = 0$ for all values of the separation d . The corresponding phase-profile can be inferred by computing $\langle e^{i\phi_k} \rangle$ for different lattice sites, after normalizing with respect to the ground-state results [Fig. 3(b)].

The situation changes dramatically for the psG model, realized by making $E_{J_1} \neq 0$ in Eq. (2), while choosing the rest of the parameters as for the sG model. Due to the perturbing potential $\sim \cos(\phi_k)$, the sG solitons and the anti-solitons experience a strong-confining potential energy, qualitatively similar to that experienced by the free, Ising domain walls under a longitudinal field [24–27]. We compute the energy-cost of separation T for the psG model as in the sG case [Fig. 3(a), filled markers]. The energy-cost grows proportional to the distance of

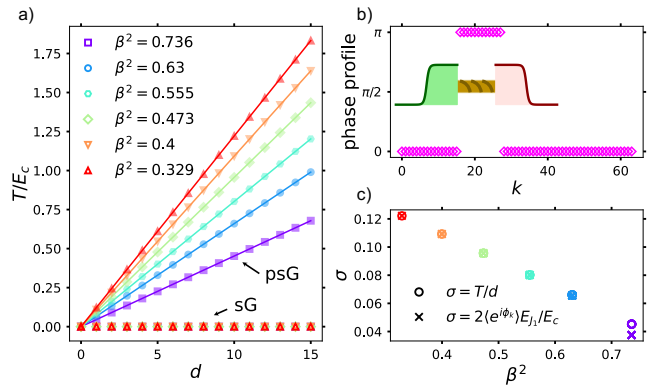


FIG. 3. a) DMRG results for the string tension for different choices of β^2 , chosen by fixing E_{J_1}/E_c [Fig. 2(c)], for $L = 64$. For the sG model (empty markers), after creating the soliton-antisoliton pair, there is no associated energy cost of separation. However, for the psG model (filled markers), due to the existence of the perturbing cosine potential $\propto E_{J_1}$ [Eq. (2)], the soliton and the anti-soliton experience a confining force. This leads to an energy cost (T/E_c) growing linearly with separation d . b) The corresponding phase-profile computed by creating a soliton-antisoliton pair and separating them by 12 lattice sites. c) The corresponding string tension, $\sigma = T/d$ (empty circles) obtained from a linear fit of the data in a). The corresponding leading-order analytical predictions for σ are denoted by crosses. The discrepancy between the predicted and obtained string-tension for $\beta^2 \approx 0.736$ occurs due to the proximity to the Kosterlitz-Thouless point ($\beta^2 = 1$).

separation: $T = \sigma d$, where σ is the string-tension. The latter is numerically obtained by fitting to this linear dependence and shown as a function of β in Fig. 3(c). To leading order, $\sigma = 2\langle e^{i\phi_k} \rangle E_{J_1}/E_c$, where the expectation value $\langle e^{i\phi_k} \rangle$ is computed for the ground state of H with $E_{J_1} = 0$. The discrepancy between the leading-order prediction and the numerical results for $\beta^2 \approx 0.736$ is due to the proximity to the Kosterlitz-Thouless point. The decrease of the string-tension with increasing β^2 can be viewed as a consequence of the increasing repulsion between the sG solitons and anti-solitons with increasing β^2 .

The spectrum of the psG model contains the newly-formed mesons and the charge-neutral sG breathers. The latter occur only for $\beta^2 < 1/2$ with their masses acquiring corrections due to the perturbing potential. Fig. 4 shows DMRG results for mass of the lightest particle as a function of the dimensionless parameter $\eta = [E_{J_1}/E_c]/[E_{J_2}/E_c]^\nu$, $\nu = (1 - \beta^2/4)/(1 - \beta^2)$, for different choices of E_{J_2}/E_c . For small η , the psG mesons are heavier (with masses $> 2M$) than the breathers (with masses $< 2M$). Thus, we compute the mass of the lightest sG breather (psG meson) for $\beta^2 < (>)1/2$. For $\eta \ll 1$, the correction to the lightest breather mass can be expanded in powers of η . We show a comparison of the obtained ratio m_b/M , m_b being the lightest sG breather mass for

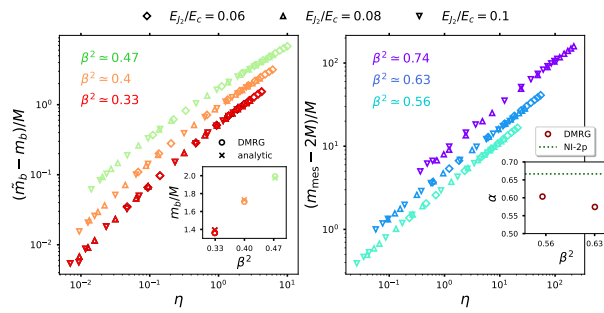


FIG. 4. DMRG results for the mass of the lightest particle of the psG model for $\beta^2 < 1/2$ (left) and $\beta^2 > 1/2$ (right), as a function of the dimensionless quantity η . Here, M (m_b) is the mass of the soliton (lightest breather) of the unperturbed sG model. The diamonds and triangles correspond to different choices of E_{J_2}/E_C . For small η , the lightest particle is the lightest sG breather (psG meson) for $\beta^2 < (>)1/2$. Using linear fit [23] of the numerical data for $\eta \ll 1$, we obtain the ratio m_b/M (comparison with the analytical prediction in the left inset). The scaling of the psG meson mass is given by: $(m_{\text{mes}} - 2M)/M \sim \eta^\alpha$ for $\eta \ll 1$. The inset in the right panel shows the comparison of the α obtained using DMRG (circles) and those using non-interacting two-particle (NI-2p) approximation (dotted line).

$\eta = 0$, with the analytical predictions in the left inset. For a comparison of our numerical data with perturbative computation [21], see [23]. For $\beta^2 > 1/2$, the spectrum contains only the psG mesons. The dependence of lowest psG meson mass is shown in Fig. 4 (right). For $\eta \ll 1$, a non-interacting two-particle (NI-2p) computation [23] predicts $(m_{\text{mes}} - 2M)/M \sim \eta^\alpha$, where $\alpha = \frac{2}{3}$. Comparison of the numerical results with the NI-2p computation is shown in the right inset. A more complete computation using the Bethe-Salpeter equation for the psG model is beyond the scope of this work.

To summarize, we have numerically demonstrated the confinement of sG solitons into mesonic bound states in a QEC array. We computed the associated string tension and computed the scaling properties of the mass of the lightest particle. It is challenging to obtain the heavier particles in the spectrum using our method (DMRG) due to the large Hilbert-space of the quantum rotors present in the QEC array. This problem can be circumvented using analog quantum simulation, where a quench experiment would be able to capture signatures of the heavier mesons. Consider the case when the junction energies of the blue Josephson junctions, E_{J_1} , in Fig. 1 are tunable. This can be accomplished by replacing the corresponding junctions by a SQUID loop with a magnetic flux threading the latter [42]. After preparing the system in the ground state of H with $E_{J_1} = 0$, the coupling E_{J_1} is turned on by tuning magnetic flux. Signatures of the confinement of the sG solitons can be obtained by probing the spectrum and the current-current correlation functions. Given the progress in the fabrication and in-

vestigation of large QEC arrays [43–45], we are optimistic of experimental vindication of our work.

Finally, we note that the QEC array for the psG model provides a robust, controllable and experimentally-realizable testbed for investigation of several other non-perturbative phenomena occurring in low-dimensional QFTs. First, the existence of multiple minima in the potential energy of the psG model makes this model suitable for quantitative investigation of false vacuum decay [46, 47]. The latter has been analyzed using semi-classical methods for the psG model [22]. A more quantitative analysis can be performed using the QEC lattice model, similar to recent works on spin-chains [48–50]. Second, tuning the form of the perturbing potential in Eq. (2) from $\cos(\phi_k)$ to $\sin(\phi_k)$, for certain values of E_{J_1}/E_{J_2} , induces a renormalization group (RG) flow from the gapped perturbed sine-Gordon model to a quantum critical point of Ising universality class [21, 22]. This can potentially lead to numerical and experimental investigation of RG flows with QEC arrays.

The authors acknowledge discussions with Johannes Hauschild, Robert Konik, Marton Kormos, Hubert Saleur, Gabor Takacs, and Yicheng Tang. AR was supported from a grant from the Simons Foundation (825876, TDN). SL was supported by NSF-PHY-2210187.

* ananda.roy@physics.rutgers.edu

† sergeil@physics.rutgers.edu

- [1] J. Greensite, *An introduction to the confinement problem*, Vol. 821 (2011).
- [2] P. Campana, M. Klute, and P. Wells, Physics goals and experimental challenges of the proton–proton high-luminosity operation of the LHC, *Annual Rev. of Nuclear and Particle Science* **66**, 273 (2016).
- [3] W. Busza, K. Rajagopal, and W. van der Schee, Heavy ion collisions: The big picture and the big questions, *Annual Rev. of Nuclear and Particle Science* **68**, 339 (2018).
- [4] B. Lake, A. M. Tsvelik, S. Notbohm, D. A. Tennant, T. G. Perring, M. Reehuis, C. Sekar, G. Krabbes, and B. Büchner, Confinement of fractional quantum number particles in a condensed-matter system, *Nature Physics* **6**, 50 (2009).
- [5] R. Coldea, D. A. Tennant, E. M. Wheeler, E. Wawrzynska, D. Prabhakaran, M. Telling, K. Habicht, P. Smeibidl, and K. Kiefer, Quantum criticality in an Ising chain: Experimental evidence for emergent E_8 symmetry, *Science* **327**, 177 (2010).
- [6] M. Kormos, M. Collura, G. Takács, and P. Calabrese, Real-time confinement following a quantum quench to a non-integrable model, *Nature Physics* **13**, 246 (2016).
- [7] J. Vovrosh, R. Mukherjee, A. Bastianello, and J. Knolle, Dynamical hadron formation in long-range interacting quantum spin chains, *PRX Quantum* **3**, 040309 (2022).
- [8] W. L. Tan, P. Becker, F. Liu, G. Pagano, K. S. Collins, A. De, L. Feng, H. B. Kaplan, A. Kyprianidis, R. Lundgren, W. Morong, S. Whitsitt, A. V. Gorshkov, and

C. Monroe, Domain-wall confinement and dynamics in a quantum simulator, *Nature Physics* **17**, 742 (2021).

[9] J. Vovrosh and J. Knolle, Confinement and entanglement dynamics on a digital quantum computer, *Scientific Reports* **11**, 11577 (2021).

[10] B. Douçot and J. Vidal, Pairing of cooper pairs in a fully frustrated Josephson-junction chain, *Phys. Rev. Lett.* **88**, 227005 (2002).

[11] L. B. Ioffe and M. V. Feigel'man, Possible realization of an ideal quantum computer in Josephson junction array, *Phys. Rev. B* **66**, 224503 (2002).

[12] A. Kitaev, Protected qubit based on a superconducting current mirror (2006), arXiv:cond-mat/0609441.

[13] P. Brooks, A. Kitaev, and J. Preskill, Protected gates for superconducting qubits, *Phys. Rev. A* **87**, 052306 (2013).

[14] S. Gladchenko, D. Olaya, E. Dupont-Ferrier, B. Douçot, L. B. Ioffe, and M. E. Gershenson, Superconducting nanocircuits for topologically protected qubits, *Nature Physics* **5**, 48 (2008).

[15] W. C. Smith, A. Kou, X. Xiao, U. Vool, and M. H. Devoret, Superconducting circuit protected by two-Cooper-pair tunneling, *NPJ Quantum Information* **6**, 8 (2020), arXiv:1905.01206 [quant-ph].

[16] A. Gyenis, P. S. Mundada, A. Di Paolo, T. M. Hazard, X. You, D. I. Schuster, J. Koch, A. Blais, and A. A. Houck, Experimental realization of a protected superconducting circuit derived from the $0-\pi$ qubit, *PRX Quantum* **2**, 010339 (2021).

[17] A. Roy and H. Saleur, Quantum electronic circuit simulation of generalized sine-Gordon models, *Phys. Rev. B* **100**, 155425 (2019).

[18] A. Roy, D. Schuricht, J. Hauschild, F. Pollmann, and H. Saleur, The quantum sine-Gordon model with quantum circuits, *Nucl. Phys. B* **968**, 115445 (2021), arXiv:quant-ph/2007.06874.

[19] D. K. Campbell, M. Peyrard, and P. Sodano, Kink-antikink interactions in the double sine-Gordon equation, *Physica D: Nonlinear Phenomena* **19**, 165 (1986).

[20] G. Delfino and G. Mussardo, Non-integrable aspects of the multi-frequency sine-Gordon model, *Nuclear Physics B* **516**, 675–703 (1998).

[21] Z. Bajnok, L. Palla, G. Takacs, and F. Wagner, Nonperturbative study of the two frequency sine-Gordon model, *Nucl. Phys. B* **601**, 503 (2001), arXiv:hep-th/0008066.

[22] G. Mussardo, V. Riva, and G. Sotkov, Semiclassical particle spectrum of double sine-Gordon model, *Nucl. Phys. B* **687**, 189 (2004), arXiv:hep-th/0402179.

[23] See supplementary material for details.

[24] P. Fonseca and A. Zamolodchikov, Ising field theory in a magnetic field: Analytic properties of the free energy, *J. Stat. Phys.* **110**, 527 (2003).

[25] S. B. Rutkevich, Large- n excitations in the ferromagnetic Ising field theory in a weak magnetic field: Mass spectrum and decay widths, *Phys. Rev. Lett.* **95**, 250601 (2005).

[26] P. Fonseca and A. Zamolodchikov, Ising spectroscopy. I. Mesons at $T < T_c$, (2006), arXiv:hep-th/0612304.

[27] S. B. Rutkevich, Energy spectrum of bound-spinons in the quantum Ising spin-chain ferromagnet, *J. Stat. Phys.* **131**, 917 (2008).

[28] A. J. A. James, R. M. Konik, and N. J. Robinson, Non-thermal states arising from confinement in one and two dimensions, *Phys. Rev. Lett.* **122**, 130603 (2019).

[29] N. J. Robinson, A. J. A. James, and R. M. Konik, Signatures of rare states and thermalization in a theory with confinement, *Phys. Rev. B* **99**, 195108 (2019).

[30] M. Goldstein, M. H. Devoret, M. Houzet, and L. I. Glazman, Inelastic microwave photon scattering off a quantum impurity in a Josephson-junction array, *Phys. Rev. Lett.* **110**, 017002 (2013).

[31] L. I. Glazman and A. I. Larkin, New quantum phase in a one-dimensional Josephson array, *Phys. Rev. Lett.* **79**, 3736 (1997).

[32] M. P. A. Fisher, P. B. Weichman, G. Grinstein, and D. S. Fisher, Boson localization and the superfluid-insulator transition, *Phys. Rev. B* **40**, 546 (1989).

[33] S. Sachdev, *Quantum Phase Transitions* (Cambridge University Press, 2011).

[34] T. Giamarchi, Mott transition in one dimension, *Physica B: Condensed Matter* **230–232**, 975 (1997), proceedings of the International Conference on Strongly Correlated Electron Systems.

[35] T. D. Kühner, S. R. White, and H. Monien, One-dimensional bose-hubbard model with nearest-neighbor interaction, *Phys. Rev. B* **61**, 12474 (2000).

[36] The DMRG computations of this work were performed using the TeNPy package [51].

[37] A. Roy, F. Pollmann, and H. Saleur, Entanglement Hamiltonian of the 1+1-dimensional free, compactified boson conformal field theory, *J. Stat. Mech.* **2008**, 083104 (2020), arXiv:cond-mat/2004.14370.

[38] F. Smirnov, *Form Factors in Completely Integrable Models of Quantum Field Theory*, Advanced series in mathematical physics (World Scientific, 1992).

[39] S. L. Lukyanov, Form-factors of exponential fields in the sine-Gordon model, *Mod. Phys. Lett. A* **12**, 2543 (1997), arXiv:hep-th/9703190.

[40] S. Mandelstam, Soliton operators for the quantized sine-Gordon equation, *Phys. Rev. D* **11**, 3026 (1975).

[41] S. Lukyanov and A. Zamolodchikov, Form factors of soliton-creating operators in the sine-Gordon model, *Nuclear Physics B* **607**, 437 (2001).

[42] M. Tinkham, *Introduction to Superconductivity: Second Edition*, Dover Books on Physics (Dover Publications, 2004).

[43] R. Kuzmin, N. Mehta, N. Grabon, R. Mencia, and V. E. Manucharyan, Superstrong coupling in circuit quantum electrodynamics, *NPJ Quantum Information* **5**, 20 (2019).

[44] S. Léger, J. Puertas-Martínez, K. Bharadwaj, R. Dassonneville, J. Delaforce, F. Foroughi, V. Milchakov, L. Planat, O. Buisson, C. Naud, W. Hasch-Guichard, S. Florens, I. Snyman, and N. Roch, Observation of quantum many-body effects due to zero point fluctuations in superconducting circuits, *Nature Communications* **10**, 5259 (2019).

[45] J. Puertas Martínez, S. Léger, N. Gheeraert, R. Dassonneville, L. Planat, F. Foroughi, Y. Krupko, O. Buisson, C. Naud, W. Hasch-Guichard, S. Florens, I. Snyman, and N. Roch, A tunable Josephson platform to explore many-body quantum optics in circuit-qed, *NPJ Quantum Information* **5**, 19 (2019).

[46] S. Coleman, Fate of the false vacuum: Semiclassical theory, *Phys. Rev. D* **15**, 2929 (1977).

[47] S. Coleman, *Aspects of Symmetry: Selected Erice Lectures* (Cambridge University Press, 1988).

[48] S. B. Rutkevich, Decay of the metastable phase in $d = 1$ and $d = 2$ Ising models, *Phys. Rev. B* **60**, 14525 (1999).

- [49] G. Lagnese, F. M. Surace, M. Kormos, and P. Calabrese, False vacuum decay in quantum spin chains, *Phys. Rev. B* **104**, L201106 (2021).
- [50] A. Milsted, J. Liu, J. Preskill, and G. Vidal, Collisions of false-vacuum bubble walls in a quantum spin chain, *PRX Quantum* **3**, 020316 (2022).
- [51] J. Hauschild and F. Pollmann, Efficient numerical simulations with Tensor Networks: Tensor Network Python (TeNPy) *SciPost Phys. Lect. Notes*, 5 (2018).

Supplementary Material: Soliton Confinement in a Quantum Circuit

Ananda Roy^{1,*} and Sergei Lukyanov^{1,†}

¹*Department of Physics and Astronomy, Rutgers University, Piscataway, NJ 08854-8019 USA*

The supplementary material is organized as follows. In Sec. I, the scaling limit of the quantum electronic circuit array is described, starting with the free-boson model, followed by the sine-Gordon (sG) and the perturbed sG (psG) models. The computation of the two-point correlation functions for the sG model is given in Sec. I B. In Sec. II, results for the ground state energy and the mass of the lightest particle in the psG model are presented. In Sec. III, some details of the density matrix renormalization group simulations, together with more numerical results obtained for the lattice models, are given.

I. SCALING LIMIT OF THE QEC LATTICE HAMILTONIAN

A. Free Boson Model

We start with a variant of the Bose-Hubbard model [1, 2] governed by the lattice Hamiltonian

$$H_0 = E_c \sum_{k=1}^L n_k^2 + \epsilon E_c \sum_{k=1}^L n_k n_{k+1} - E_J \sum_{k=1}^L \cos(\phi_k - \phi_{k+1}) - E_g \sum_{k=1}^L n_k \quad (\text{I.1})$$

with¹

$$[n_j, e^{\pm i\phi_k}] = \pm \delta_{jk} e^{\pm i\phi_k}.$$

The system has been analyzed analytically in Ref. [3] (see also Ref. [4] for the $\epsilon = 0$ case) and numerically using the DMRG technique in Ref. [5]. For $E_J \ll E_c$, it can be either in a Mott-insulating phase with integer filling or in a charge-density-wave phase with half-integer filling (see Appendix B of Ref. [5] for the phase-diagram). Here, we focus on the case when the insulating phase has a density of Cooper-pairs is 1/2. For $\epsilon = 0.2$, this is achieved by tuning the gate voltage $E_g/E_c = 1.2$. In this case, as E_J/E_c increases from zero, for $E_J/E_c > 0.09$, the system becomes critical and its low-energy properties can be explored within conformal field theory (see Ref. [5] for details).

In the case of a critical lattice system subject to (quasi) periodic boundary conditions, conformal invariance predicts a so-called tower structure for the low-energy spectrum [6]. Each conformal tower is labeled by a pair of conformal dimensions $(\Delta, \bar{\Delta})$ while excitations inside the tower are characterized by a non-negative integers (N, \bar{N}) . Denoting the excitation energy over the ground state by ΔE and the corresponding momenta by P , the energy-momentum spectrum of states from the conformal tower is described as

$$\Delta E = \frac{2\pi E_c}{L} u (\Delta + \bar{\Delta} + N + \bar{N}) + o(1/L) \quad (\text{I.2})$$

$$P = \frac{2\pi E_c}{L} (\Delta - \bar{\Delta} + N - \bar{N}). \quad (\text{I.3})$$

Assuming that ϵ and E_g/E_c are fixed as above, the ‘‘Fermi velocity’’ u is a certain function of dimensionless ratio E_J/E_c [see Fig. 3(a)].

The field theory underlining the critical behavior of the lattice system [Eq. (I.1)] is the Gaussian model defined by the Euclidean action

$$\mathcal{A}_0 = \frac{1}{2\pi K} \int d^2x [(\partial_\tau \phi)^2 + (\partial_x \phi)^2]. \quad (\text{I.4})$$

In the condensed matter terminology, K is called the Luttinger parameter, which is a function of E_J/E_c [see Fig. 4(b)]. Since the length scale $1/E_c$ can be naturally identified with the lattice spacing, the integer k labeling the lattice sites in Eq. (I.1) and ‘‘physical’’ time t are related to the Euclidean coordinates (x, τ) as

$$x = k/E_c, \quad \tau = -iut/E_c. \quad (\text{I.5})$$

* ananda.roy@physics.rutgers.edu

† sergeil@physics.rutgers.edu

¹ In what follows we use a system of units with $\hbar = c = 1$, so that all energy scales have dimension [length]⁻¹.

B. The sine-Gordon model

Consider a perturbation of the Hamiltonian in Eq. (I.1):

$$H_1 = H_0 - E_{J_2} \sum_{k=1}^L \cos(2\phi_k). \quad (\text{I.6})$$

The corresponding (renormalized) Euclidean action takes the form

$$\mathcal{A}_{\text{sG}} = \int d^2x \left[\frac{1}{16\pi} \partial_\nu \varphi \partial^\nu \varphi - 2\mu \cos(\beta\varphi) \right]. \quad (\text{I.7})$$

Here, instead of the Luttinger parameter K , we use the dimensionless coupling constant

$$\beta = \sqrt{K/2}, \quad 0 < \beta < 1 \quad (\text{I.8})$$

and

$$\varphi = \phi \sqrt{8/K}. \quad (\text{I.9})$$

The lattice energy scale E_c plays the role of the cut-off energy, while E_{J_2} in Eq. (I.6) is a bare coupling constant. In the scaling limit, $E_c \rightarrow \infty$ while the combination $E_{J_2}E_c^{1-2\beta^2}$ is kept fixed. To assign a precise meaning to the renormalized coupling μ , one should impose a normalization condition on the renormalized field $\cos(\beta\varphi)$. The latter has the scale dimension $d = 2\beta^2$ and is normalized by the condition

$$\lim_{r \rightarrow 0} r^{2d} \langle \cos(\beta\varphi)(x_1) \cos(\beta\varphi)(x_2) \rangle = \frac{1}{2} \quad (r \equiv |x_1 - x_2|). \quad (\text{I.10})$$

Then,

$$\mu = C E_{J_2} E_c^{1-2\beta^2}, \quad (\text{I.11})$$

where the constant C depends on the dimensionless coupling β (see also Fig. 4). A remarkable feature of the model of Eq. (I.6) is that the scaling behavior occurs already for $E_{J_2}/E_c \lesssim 1$ for all $\beta^2 \in (0, 1)$. To illustrate this, we consider two-point correlation functions of exponential fields.

Short distance expansion

Among local fields of the sine-Gordon model, a special role belongs to the exponential operators $e^{i\alpha\varphi}$. The short distance expansion of the two-point correlator of such fields was discussed in Ref. [7]. However, results of this work for the correlation function

$$\mathcal{G}_{\alpha_1, \alpha_2}(r) = \langle e^{i\alpha_1\varphi}(x_1) e^{i\alpha_2\varphi}(x_2) \rangle \quad (\text{I.12})$$

can be applied literally for $\alpha_1 + \alpha_2 \neq 0$ only. Here, we are focusing on the case when $\alpha_2 = -\alpha_1 = \alpha$. The required small- r expansion can be obtained from Eq. (2.23) from Ref. [7] through a certain limiting procedure. Below, we describe few leading terms of the short distance expansion of

$$\mathcal{G}_{-\alpha, \alpha}(r) = \langle e^{-i\alpha\varphi}(x_1) e^{i\alpha\varphi}(x_2) \rangle, \quad (\text{I.13})$$

which is applicable to the case

$$|\alpha| \leq \beta$$

for generic values of $\beta \in (0, 1)$. Similar to Eq. (I.10), we fix the normalization of the exponential fields by the condition

$$\lim_{r \rightarrow 0} r^{4\alpha^2} \mathcal{G}_{-\alpha, \alpha}(r) = 1.$$

Then it is possible to show that

$$r^{4\alpha^2} \mathcal{G}_{-\alpha, \alpha}(r) = 1 + J(2\alpha\beta, -2\beta^2) \mu^2 r^{4(1-\beta^2)} - \frac{1}{4} \alpha^4 \mathcal{H}(0) r^4 + \mu r^2 \mathcal{G}_\beta \quad (\text{I.14})$$

$$\times \left[2S(2\alpha\beta) - (4\alpha\beta)^2\pi \log(r) - (2\alpha\beta)^2\pi \frac{\partial}{\partial\beta^2} \log(\mathcal{G}_\beta) \Big|_\mu \right] + O\left(r^6, r^{8(1-\beta^2)}, r^{4(1+\beta^2)}\right) \right] .$$

The formula calls for some remarks. Firstly, the symbol for the remaining term stands for

$$O(r^a, r^b, r^c) \equiv O(r^d) \quad \text{where } d = \min(a, b, c) - \epsilon \quad \forall \epsilon > 0 .$$

For explanation of the terms in Eq. (I.14), we refer the reader to Refs. [7, 8]. The expansion coefficients read explicitly:

(i)

$$J(a, c) = A(a, c) + 2B(a, c) + C(a, c) \quad (\text{I.15})$$

with

$$A(a, c) = (1 - \cos(\pi c) \cos(\pi(2a + c)))$$

$$\times \left[a\Gamma(1-a)\Gamma(1+a+c)\Gamma(-1-c) {}_3F_2^2(-c, -1-c, 1-a; -a-c, 2; 1) \right]^2 ,$$

$$B(a, c) = \frac{a^2 \pi^2 \Gamma(1+c) \Gamma(-1-a-c)}{(1+a+c)(2+a+c)\Gamma(-a)} {}_3F_2(-c, -1-c, 1-a; -a-c, 2; 1)$$

$$\times {}_3F_2(a, 1+a, 2+c; 2+a+c, 3+a+c; 1)$$

and

$$C(a, c) = -\frac{\Gamma(-1-a-c)\Gamma(-2-a-c)}{\Gamma(2+a+c)\Gamma(3+a+c)}$$

$$\times \left[\frac{\Gamma(1+a)}{\Gamma(-a)} \frac{\pi\Gamma(2+c)}{\Gamma(-c)} {}_3F_2(a, 1+a, 2+c; 2+a+c, 3+c+a; 1) \right]^2 .$$

Here ${}_3F_2(a_1, a_2, a_3; c_1, c_2; z)$ is the conventional generalized hypergeometric function at $z = 1$. It should be pointed out that the definition (I.15) is literally applicable for $|\alpha| < \beta$. The individual terms in its r.h.s. diverges as $|\alpha| \rightarrow \beta$. Nevertheless the sum remains finite at $|\alpha| = \beta$.

(ii)

$$S(a) = -a^2\pi [\psi(1+a) + \psi(1-a) + 2\gamma_E - 2] ,$$

where $\psi(z) = \partial_z \log \Gamma(z)$ and γ_E stands for the Euler constant.

(iii) Functions

$$\mathcal{G}_\beta = \frac{1}{2} (1+\xi) \frac{\Gamma(\frac{\xi}{2})}{\Gamma(1-\frac{\xi}{2})} \frac{\Gamma(\frac{1}{2}-\frac{\xi}{2})}{\Gamma(\frac{1}{2}+\frac{\xi}{2})} \left(\frac{\Gamma(1-\beta^2)}{\Gamma(\beta^2)} \right)^{1+\xi} (\pi\mu)^\xi$$

and

$$\mathcal{H}(0) = -\frac{16}{\pi^{\frac{3}{2}} \Gamma^3(\frac{3}{2} + \frac{\xi}{2})} \left[\frac{\Gamma(\frac{\xi}{2})}{\Gamma(1-\frac{\xi}{2})} \frac{\Gamma(\frac{1}{2}-\frac{\xi}{2})}{\Gamma(\frac{1}{2}+\frac{\xi}{2})} \right]^2 \left(\frac{\Gamma(1-\beta^2)}{\Gamma(\beta^2)} \right)^{2(1+\xi)} (\pi\mu)^{2+2\xi} .$$

In the last formulae we use the so-called renormalized coupling constant which is related to β as

$$\xi = \frac{\beta^2}{1-\beta^2} . \quad (\text{I.16})$$

Long distance expansion

The correlation function in Eq. (I.13) admits the large distance expansion in terms of the exact form-factors [9, 10]. The leading term corresponds to the zero-particle contribution, i.e., a vacuum expectation value of the exponential fields:

$$\lim_{r \rightarrow +\infty} \mathcal{G}_{-\alpha, \alpha}(r) = \mathcal{G}_\alpha^2, \quad \mathcal{G}_\alpha = \langle e^{\pm i\alpha\phi} \rangle.$$

The latter was found in Ref. [11],

$$\mathcal{G}_\alpha = \left[\pi \mu \frac{\Gamma(1 - \beta^2)}{\Gamma(\beta^2)} \right]^{\frac{\alpha^2}{1 - \beta^2}} \exp \left(\int_0^\infty \frac{dt}{t} \left(\frac{\sinh^2(2\alpha\beta t)}{2 \sinh(\beta^2 t) \sinh(t) \cosh((1 - \beta^2)t)} - 2\alpha^2 e^{-2t} \right) \right). \quad (\text{I.17})$$

The particle spectrum of the sG model contains a soliton-antisoliton doublet with the same mass M . A relation between M and the dimensionfull coupling μ from the renormalized action Eq. (I.7) is known after the work [12],

$$\mu = \frac{\Gamma(\beta^2)}{\pi \Gamma(1 - \beta^2)} \left[\frac{\sqrt{\pi} \Gamma(\frac{1}{2} + \frac{\xi}{2})}{2 \Gamma(\frac{\xi}{2})} M \right]^{2 - 2\beta^2}. \quad (\text{I.18})$$

Here, together with β^2 , we use again the renormalized coupling ξ of Eq. (I.16).

If the dimensionless coupling β is restricted to the domain

$$\frac{1}{2} \leq \beta^2 < 1,$$

all the particles repell each other and no bound states are formed. In this case, the two leading terms corresponding to zero- and two- particle contributions to the correlator in Eq. (I.13) can be written in the form

$$\mathcal{G}_{-\alpha, \alpha}(r) = \mathcal{G}_\alpha^2 \left(1 + \frac{1}{2\pi^2} \int_{-\infty}^{+\infty} d\theta |f_\alpha(\theta + i\pi)|^2 \cosh\left(\frac{\theta}{\xi}\right) K_0\left(2Mr \cosh\left(\frac{\theta}{2}\right)\right) + \dots \right),$$

where ovals stand for the four- and higher-particle contributions. The analytical form of $f_\alpha(\theta)$, which is a meromorphic function of the rapidity variable θ , was presented (in slightly different notations) in the work [13]. It is considerably simpler for $\alpha = \beta$ and $\alpha = \beta/2$ than for generic values of α [10, 13]:

$$f_\beta(\theta) = \frac{2}{\xi} \cot\left(\frac{\pi\xi}{2}\right) \frac{\theta \cosh\left(\frac{\theta}{2}\right)}{\sinh\left(\frac{\theta}{\xi}\right)} \exp \left[- \int_0^\infty dt \frac{\sin^2\left(\frac{t\theta}{\pi}\right)}{t \sinh(2t)} \left(\frac{\sinh(t(\xi - 1))}{\cosh(t) \sinh(t\xi)} - 2 e^{-2t} \right) \right],$$

while

$$f_{\beta/2}(\theta) = \frac{\theta \coth\left(\frac{\theta}{2}\right)}{\xi \sinh\left(\frac{\theta}{\xi}\right)} \exp \left[- \int_0^\infty dt \frac{\sin^2\left(\frac{t\theta}{\pi}\right)}{t \sinh(2t)} \left(\frac{\sinh(t(\xi - 1))}{\cosh(t) \sinh(t\xi)} - 2 e^{-2t} \right) \right].$$

Here $K_\nu(x)$ is the conventional modified Bessel function of the second kind.

In the parameter domain

$$0 < \beta^2 < \frac{1}{2},$$

the soliton-antisoliton pair form bounded states – the breathers. The mass of the lightest breather, m_b , is simply related to the soliton mass:

$$m_b = 2M \sin\left(\frac{\pi\xi}{2}\right).$$

In the case

$$\frac{1}{3} < \beta^2 < \frac{1}{2},$$

this is the only bound state and the one-particle contribution to the correlation function $\mathcal{G}_{-\alpha, \alpha}(r)$ is given by

$$\mathcal{G}_{-\alpha, \alpha}^{(1\text{-part})}(r) = \left[\frac{2 \sin(\pi \alpha \sqrt{\xi(1+\xi)})}{\pi \sqrt{\xi(1+\xi)}} \right]^2 Z K_0(m_b r) .$$

Here Z is the so-called wave-function renormalization constant [14]

$$Z = \frac{\pi \xi(1+\xi)}{2 \sin(\frac{\pi \xi}{2})} \exp \left(- \int_0^{\pi \xi} \frac{dt}{\pi} \frac{t}{\sin(t)} \right) .$$

A comparison of the analytical predictions with the DMRG results is presented in Fig. 2 of the main text.

C. The perturbed sine-Gordon model

Now, consider the Hamiltonian

$$H_2 = H_1 - E_{J_1} \sum_{k=1}^L \cos(\phi_k) = H_0 - E_{J_2} \sum_{k=1}^L \cos(2\phi_k) - E_{J_1} \sum_{k=1}^L \cos(\phi_k) . \quad (\text{I.19})$$

The corresponding action takes the form

$$\mathcal{A}_{\text{psG}} = \int d^2x \left[\frac{1}{16\pi} \partial_\nu \varphi \partial^\nu \varphi - 2\mu \cos(\beta\varphi) - 2\lambda \cos(\beta\varphi/2) \right] , \quad (\text{I.20})$$

where the field $\cos(\beta\varphi/2)$ with scale-dimension $\beta^2/2$ is normalized similarly as in Eq. (I.10). In terms of the bare couplings of the Hamiltonian in Eq. (I.19),

$$\lambda = C' E_{J_1} E_c^{1-\beta^2/2} , \quad (\text{I.21})$$

where C' is a function of E_{J_1}/E_{J_2} and the Luttinger parameter. We use the dimensionless parameter

$$\eta = \frac{E_{J_1}/E_c}{(E_{J_2}/E_c)^\nu} , \quad \nu = \frac{1-\beta^2/4}{1-\beta^2} . \quad (\text{I.22})$$

This is expressed in terms of the renormalized couplings as:

$$\eta = \frac{C'}{C^\nu} \frac{\lambda}{\mu^\nu} , \quad (\text{I.23})$$

where C and C' are β -dependent constants [see Eqs. (I.11, I.21)].

II. GROUND STATE ENERGY AND MASS OF THE LIGHTEST PARTICLE IN THE PERTURBED SINE-GORDON MODEL

In this section, we present the results for the ground state energy and the mass of the lightest particle in the psG model and compare with analytical predictions.

A. Ground state energy

The change in ground state energy density \mathcal{E} of the psG model with respect to the sG model, is given, in general, by

$$\mathcal{E}_{\text{psG}} - \mathcal{E}_{\text{sG}} = M^2 G(\eta) , \quad (\text{II.1})$$

where the function $G(\eta)$ admits an expansion in a Taylor series in $\eta \sim \lambda$. To leading order in the perturbation theory,

$$\mathcal{E}_{\text{psG}} - \mathcal{E}_{\text{sG}} = -2\lambda \mathcal{G}_{\beta/2} + O(\lambda^2) , \quad (\text{II.2})$$

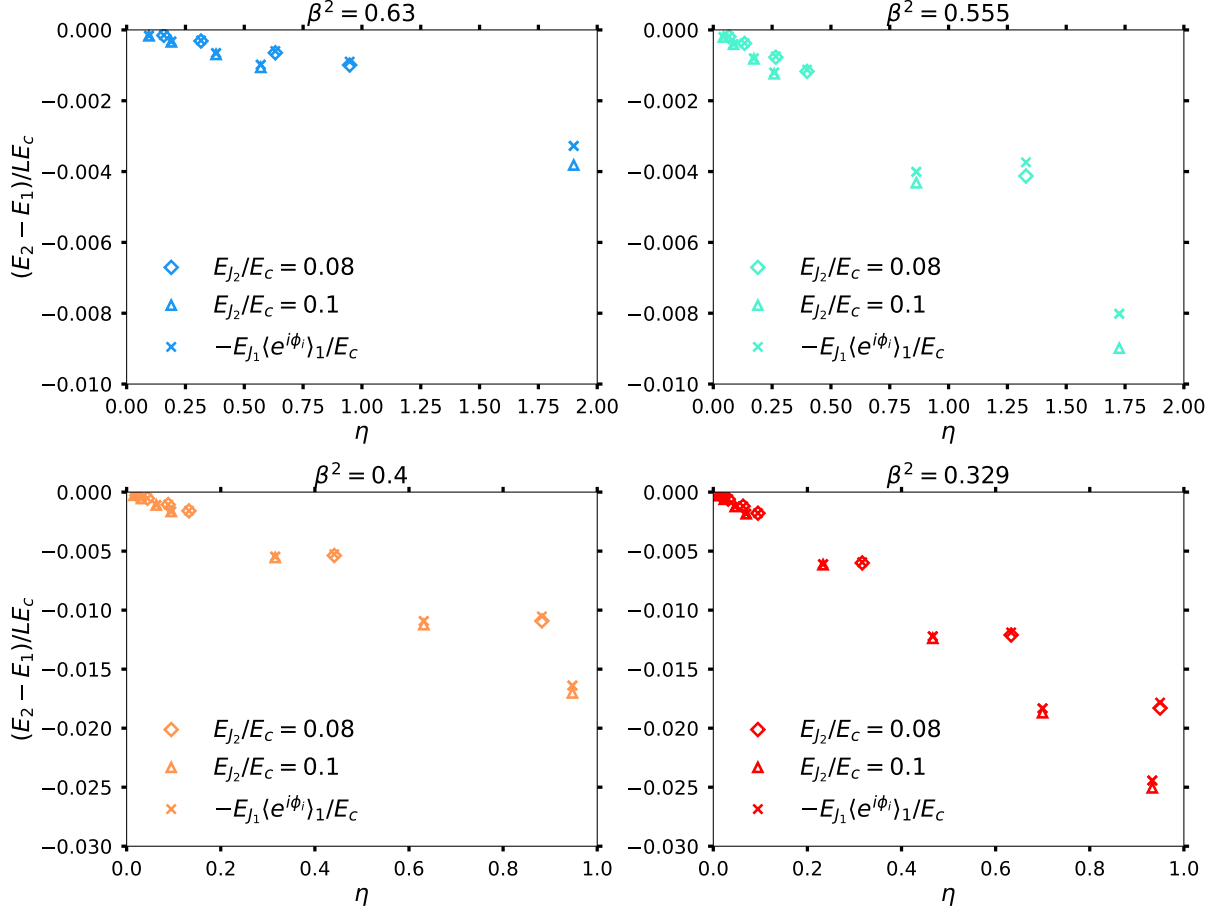


FIG. 1. Comparison of the change in the ground state energy density for the lattice model in Eq. (I.19) with respect to that in Eq. (I.6) for different choices of β^2 as a function of the dimensionless parameter η [see Eq. (I.22)]. The triangular markers correspond to different choices of lattice coupling E_{J_2}/E_c . The corresponding analytical predictions are shown as crosses.

where $\mathcal{G}_{\beta/2}$ is the expectation value of the operator $e^{i\beta\varphi/2}$, given by Eq. (I.17). For the lattice model, the corresponding first-order correction to energy, in units of E_c , is given by

$$\frac{E_2 - E_1}{LE_c} = -\frac{E_{J_1}}{E_c} \langle e^{i\phi_i} \rangle_1 + O(E_{J_1}^2/E_c^2), \quad (\text{II.3})$$

where the expectation value is taken in the ground state of H_1 . A comparison of this prediction with DMRG results for the ground state energy for the lattice model of Eq. (I.19) is shown in Fig. 1. Expectedly, the DMRG results are compatible with the perturbative prediction for smaller values of η .

B. Correction to the mass of the lightest sG breather

The $\cos(\beta\varphi/2)$ perturbation of the psG model induces corrections to the masses of the breathers that exist in the original sG model for $\beta^2 < 1/2$. To the first perturbative order, the difference between the breather mass \tilde{m}_b in the psG model and that in the sG model is:

$$\frac{\tilde{m}_b - m_b}{M} = D\lambda + O(\lambda^2) \quad (\text{II.4})$$

and the coefficient D was computed within “one-particle approximation” in Ref. [15]. The formula given in Eq. (5.13) of that paper can be simplified to

$$D \approx \frac{2\mathcal{G}_{\beta/2}}{M^2 \cos(\pi\xi/2)}, \quad (\text{II.5})$$

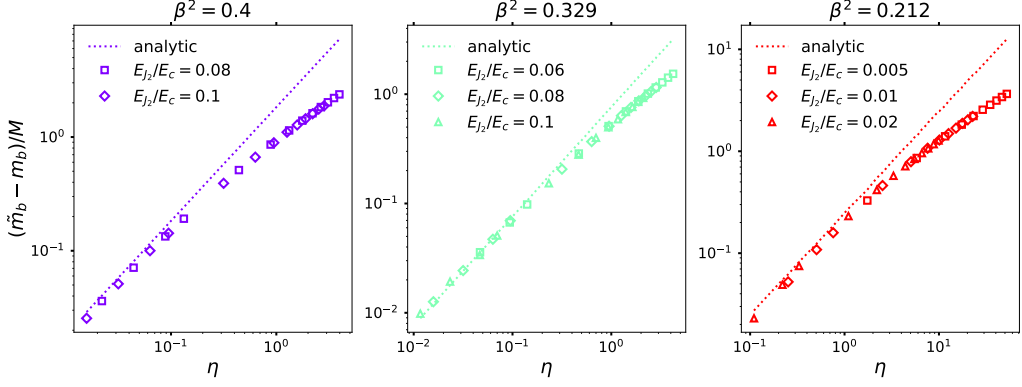


FIG. 2. Comparison of the analytical predictions computed within the one-particle approximation with the DMRG computation as a function of η [Eq. (I.22)] for three choices of β^2 .

where ξ, M are defined in Eq. (I.16) and Eq. (I.18) respectively. In terms of the lattice parameters, the leading-order correction to the breather mass can be rewritten as

$$\frac{\tilde{m}_b - m_b}{M} \approx \frac{1}{u^3 \cos(\pi \xi/2)} \left(\frac{E_c}{M} \right)^2 \frac{E_{J1}}{E_c} \langle e^{i\phi_i} \rangle_1. \quad (\text{II.6})$$

A comparison of this analytical result (dotted line) with our numerical data (squares, diamonds and triangles) is given in Fig. 2. The lowest-order predictions work well for $\beta^2 \ll 1/2$ even for $\eta \sim 1$. As β^2 approaches 1/2, it is expected that the corrections from the higher particle contributions become important. Nevertheless, the agreement between the DMRG and analytical results is still reasonable.

C. Scaling of the mesons masses in the perturbed sine-Gordon model

For $\beta^2 = 1/2$, the psG model is equivalent to the non-interacting, massive Dirac fermion theory, perturbed by the $\cos(\beta\varphi/2)$ potential. For this case, following Ref. [16] (see also Refs. [17, 18]), the masses of the mesons can be approximately computed using the quantum mechanical Hamiltonian for the soliton and antisoliton pair:

$$H_{\text{NI-2p}} = \frac{p_1^2}{2M} + \frac{p_2^2}{2M} + \sigma|x_1 - x_2|. \quad (\text{II.7})$$

Here, M is soliton mass and $\sigma = 2\lambda \langle e^{i\beta\varphi/2} \rangle$ is the string tension within this approximation [see Fig. 3 of main text for numerical results for σ]. The masses of the mesons, to leading order, are determined by the zeros of the Airy function z_n , $n = 1, 2, \dots$:

$$m_n = 2M + \left(\frac{\sigma^2}{M} \right)^{1/3} z_n. \quad (\text{II.8})$$

In terms of the dimensionless parameter η [see Eq. (I.22)], for small η , one has

$$\frac{m_n - 2M}{M} \propto \eta^{2/3} \quad (\eta \ll 1). \quad (\text{II.9})$$

Strictly-speaking, this formula holds true only for $\beta^2 = 1/2$. In general, the small- η behavior is described by an exponent α that depends on β (see Fig. 4 of the main text). The computation of this exponent is an interesting open problem which would require inclusion of the soliton-antisoliton interaction.

III. NOTES ON DMRG SIMULATION

Next, we provide details of the numerical simulations performed using DMRG, building on the setup developed in Refs. [5, 19].

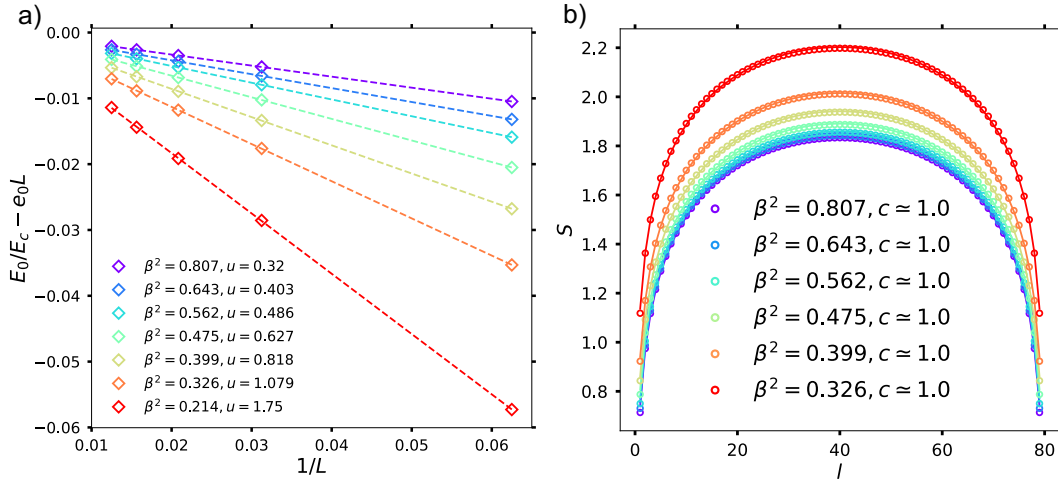


FIG. 3. DMRG results for the Fermi velocity (u) and the central charge (c) for the free boson model.

At each lattice site, we define a quantum rotor in the occupation basis: $\{|n_k\rangle\}$, where n_k -s range from -8 to $+8$ in steps of 1 . This leads to a local Hilbert space with dimension 17 . This truncation was sufficient to get the accurate and stable data for the half-filling case analyzed in this work. Note that the Hilbert space is larger than that of the earlier works. This is because of the existence of the $\cos(2\phi_k)$ term in Eq. (I.1), which necessitates a doubling of the local Hilbert space dimension. The lattice vertex operators can be straightforwardly defined based on their action on the basis states [19]. The simulations were done using the single-site DMRG routine of the TeNPy package [20].

The free boson model

To characterize the free-boson phase, we set $E_{J_1} = E_{J_2} = 0$ and $E_g/E_c = 1.2$ [see discussion below Eq. (I.1)]. The Luttinger parameter K is computed by calculating the two-point correlation function of the $e^{i\phi_k}$ operator in the ground-state obtained using infinite DMRG technique [see Fig. 2(a) of the main text]. The velocity of light, u , is obtained by computing the scaling of the ground-state energy with system size using the conformal field theory prediction for periodic boundary conditions [6]:

$$\frac{E_0}{E_c} = e_0 L - \frac{\pi c u}{6L} + o(1/L), \quad (\text{III.1})$$

where the two terms on the r.h.s respectively correspond to the extensive and Casimir contributions to the energy. The central charge c is independently verified to be 1 by using the scaling of the entanglement entropy with the subsystem size [21, 22]:

$$S(l) = \frac{c}{3} \ln \left[\frac{L}{\pi} \sin \left(\frac{\pi l}{L} \right) \right] + S_0, \quad (\text{III.2})$$

where l is the subsystem size, S_0 is a non-universal contribution to the entanglement entropy. We compute the Fermi velocity by varying the system size as $L = 16p$, $p = 1, 2, \dots, 5$ [see Fig. 3(a)]. The corresponding results for the entanglement entropy are shown in Fig. 3(b).

The sine-Gordon model

The ground state of the Hamiltonian H_1 , [Eq. (I.6)], was computed by conserving the \mathbb{Z}_2 charge associated with the parity of the Cooper-pair number: $P = \prod_{j=1}^L e^{i\pi n_j}$. Let the two eigenstates with parity eigenvalues ± 1 be denoted by $|\psi_{\pm}\rangle$. For each of these states, $\langle \psi_{\pm} | e^{i\phi_j} | \psi_{\pm} \rangle = 0$ since the operator $e^{i\phi_j}$ change the parity sector. Diagonalizing $P_{ab} = \langle \psi_a | P | \psi_b \rangle$, where $a, b = \pm$, gives the eigenstates of $e^{i\phi_j}$, which become the symmetry-broken ground states of the sG model in the scaling limit.

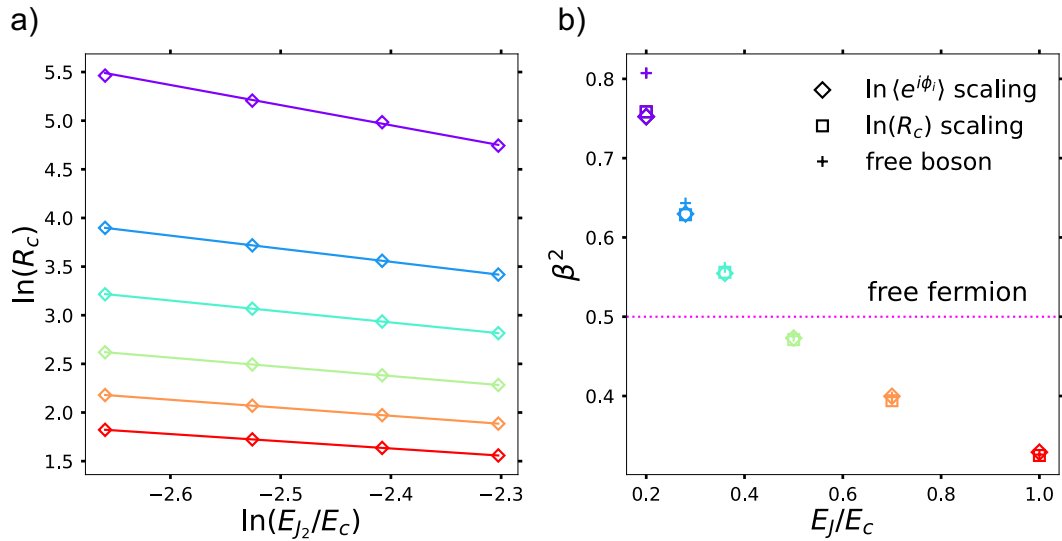


FIG. 4. DMRG results for the variation of the correlation length R_c with the coupling E_{J_2}/E_c and the comparison with the values of $\beta^2 = K/2$ obtained from the Luttinger parameter K of the free boson theory and the scaling of the vertex operator $e^{i\phi_k}$ (see also Fig. 2 of the main text). Note that the results for the correlation length, together with Eqs. (I.18, III.3), provide a numerical estimate of the non-universal constant C of Eq. (I.11).

To minimize finite size effects in the computation of the correlation functions, the infinite DMRG technique was used. To obtain the soliton mass, the correlation length R_c of the matrix product state was computed. The numerical results for R_c were converged to the three significant figures. In the parameter domain $1/4 < \beta^2 < 1$, the soliton mass is expressed in terms of the correlation length as

$$M = \frac{E_c}{uR_c}. \quad (\text{III.3})$$

For $\beta^2 < 1/4$, in the above formula, M should be replaced by the mass of the lightest bound state. In the scaling limit,

$$R_c \propto \left(\frac{E_{J_2}}{E_c} \right)^{-1/(2-2\beta^2)}. \quad (\text{III.4})$$

The dependence of R_c with the ratio E_{J_2}/E_c is depicted in Fig. 4. From this, one can extract the value of the dimensionless coupling β^2 . A comparison of the values of β^2 so-obtained with those found using the other methods is shown in Fig. 4(b) (see also Fig. 2 of the main text).

The perturbed sine-Gordon model

To obtain the results for the psG model, the Hamiltonian in Eq. (I.19) with $E_{J_1}, E_{J_2} \neq 0$ was analyzed. For the computation of the string tension, a soliton-antisoliton pair is created one lattice site apart by applying the soliton creating operators, described in the main text. The expectation value of the lattice Hamiltonian in the state with the soliton-antisoliton pair one lattice site apart was taken as a reference energy.

[1] M. P. A. Fisher, P. B. Weichman, G. Grinstein, and D. S. Fisher, Boson localization and the superfluid-insulator transition, *Phys. Rev. B* **40**, 546 (1989).
[2] S. Sachdev, *Quantum Phase Transitions* (Cambridge University Press, 2011).
[3] L. I. Glazman and A. I. Larkin, New quantum phase in a one-dimensional Josephson array, *Phys. Rev. Lett.* **79**, 3736 (1997).

- [4] R. M. Bradley and S. Doniach, Quantum fluctuations in chains of Josephson junctions, *Phys. Rev. B* **30**, 1138 (1984).
- [5] A. Roy, F. Pollmann, and H. Saleur, Entanglement Hamiltonian of the 1+1-dimensional free, compactified boson conformal field theory, *J. Stat. Mech.* **2008**, 083104 (2020), arXiv:cond-mat/2004.14370.
- [6] P. Francesco, P. Di Francesco, P. Mathieu, D. Sénéchal, and D. Senechal, *Conformal Field Theory*, Graduate Texts in Contemporary Physics (Springer, 1997).
- [7] V. Fateev, D. Fradkin, S. Lukyanov, A. Zamolodchikov, and A. Zamolodchikov, Expectation values of descendent fields in the sine-Gordon model, *Nucl. Phys. B* **540**, 587 (1999).
- [8] B. Doyon and S. Lukyanov, Fermion Schwinger's function for the SU(2)-Thirring model, *Nucl. Phys. B* **644**, 451 (2002).
- [9] B. Berg, M. Karowski, and P. Weisz, Construction of Green's functions from an exact S-matrix, *Phys. Rev. D* **19**, 2477 (1979).
- [10] F. Smirnov, *Form Factors in Completely Integrable Models of Quantum Field Theory*, Advanced series in mathematical physics (World Scientific, 1992).
- [11] S. L. Lukyanov and A. B. Zamolodchikov, Exact expectation values of local fields in quantum sine-Gordon model, *Nucl. Phys. B* **493**, 571 (1997), arXiv:hep-th/9611238.
- [12] Al. B. Zamolodchikov, Mass scale in the sine-Gordon model and its reductions, *Int. J. Mod. Phys.* **10**, 1125 (1995).
- [13] S. L. Lukyanov, Form-factors of exponential fields in the sine-Gordon model, *Mod. Phys. Lett. A* **12**, 2543 (1997), arXiv:hep-th/9703190.
- [14] M. Karowski and P. Weisz, Exact form-factors in (1+1)-dimensional field theoretic models with soliton behavior, *Nucl. Phys. B* **139**, 455 (1978).
- [15] Z. Bajnok, L. Palla, G. Takacs, and F. Wagner, Nonperturbative study of the two frequency sine-Gordon model, *Nucl. Phys. B* **601**, 503 (2001), arXiv:hep-th/0008066.
- [16] B. M. McCoy and T. T. Wu, Two-dimensional Ising field theory in a magnetic field: Breakup of the cut in the two-point function, *Phys. Rev. D* **18**, 1259 (1978).
- [17] P. Fonseca and A. Zamolodchikov, Ising field theory in a magnetic field: Analytic properties of the free energy, *J. Stat. Phys.* **110**, 527 (2003).
- [18] P. Fonseca and A. Zamolodchikov, Ising spectroscopy. I. Mesons at $T < T_c$, (2006), arXiv:hep-th/0612304.
- [19] A. Roy, J. Hauschild, and F. Pollmann, Quantum phases of a one-dimensional majorana-bose-hubbard model, *Phys. Rev. B* **101**, 075419 (2020).
- [20] J. Hauschild and F. Pollmann, Efficient numerical simulations with Tensor Networks: Tensor Network Python (TeNPy), *SciPost Phys. Lect. Notes*, **5** (2018).
- [21] C. Holzhey, F. Larsen, and F. Wilczek, Geometric and renormalized entropy in conformal field theory, *Nucl. Phys. B* **424**, 443 (1994).
- [22] P. Calabrese and J. Cardy, Entanglement entropy and quantum field theory, *J. Stat. Mech: Theory and Experiment* **2004**, P06002 (2004).